energies

MDPI

Article

A Knock-Limited Otto Reference for Fuel–Engine Realization Diagnostics in Gaseous-Fueled Spark-Ignition Engines

Juan Pablo Gómez Montoya [1,*], Daniel B. Olsen [2], Yoisdel Castillo Alvarez [3,*], Johann Alexis Chávez García [3], Luis Enrique Quispe Gallegos [1], Pedro Bryan Ivarrola Granados [1] and Waldir Eloy De La Cruz Felipe [1]

[1] Department of Mechanical Engineering, Universidad Tecnológica del Perú, Lima 15046, Peru; c26731@utp.edu.pe (L.E.Q.G.); u19212137@utp.edu.pe (P.B.I.G.); u17105798@utp.edu.pe (W.E.D.L.C.F.)
[2] Department of Mechanical Engineering, Colorado State University, Fort Collins, CO 80523, USA; daniel.olsen@colostate.edu
[3] Environmental Engineering Career, Engineering Faculty, Universidad Peruana de Ciencias Aplicadas (UPC), Lima 15023, Peru; u20191e635@upc.edu.pe
* Correspondence: jgomezmo@utp.edu.pe (J.P.G.M.); pcigycas@upc.edu.pe (Y.C.A.)

Abstract

Gaseous-fueled spark-ignition engines need diagnostics that separate fuel knock resistance, the ideal thermodynamic opportunity it enables and the fraction an engine realizes. A previously proposed methane-normalized fuel factor, X_{fMN}, forced methane to unity, whereas its measured realization ratio is 0.544. This work reformulates X_{fMN} as the ratio between the measured electrical efficiency at the knock threshold and a knock-limited Otto reference built from the methane number, the critical compression ratio of a Cooperative Fuel Research (CFR) engine and the specific-heat ratio of the fuel gas. Nine fuels from a biogas spark-ignition (BSI) campaign were reanalyzed on a corrected thermochemical basis; a reconstructed 84-record matrix served only to delimit the applicability domain. A two-descriptor model based on the hydrogen-to-carbon ratio and the specific-heat ratio is identifiable, whereas the full five-descriptor model is not. Under the nominal methane-number assignment, the reduced model lowers the leave-one-out error of electrical efficiency prediction by a factor of 2.10 relative to a null model; this advantage disappears if composition-consistent methane numbers are assigned to five engine blends. Only 23 of 84 records lie inside the calibration domain, and 58 require extrapolation. X_{fMN} is therefore a local domain-aware realization diagnostic, not a universal fuel-quality ranking, and it can support fuel matching in adaptive multifuel engines.

Keywords: methane number; knock-limited Otto cycle; spark-ignition engines; biogas; hydrogen-enriched blends; critical compression ratio; identifiability; applicability domain; realization factor

Check for updates

Academic Editors: Oscar Vento and Alessandro Ferrari

Received: 29 August 2026
Revised: 12 October 2026
Accepted: 16 October 2026
Published: 9 November 2026

Copyright: © 2026 by the authors. Licensee MDPI, Basel, Switzerland. This article is an open access article distributed under the terms and conditions of the Creative Commons Attribution (CC BY) license.

1. Introduction

1.1. From Gaseous-Fuel Knock Rating to Engine-Design Variables

Spark-ignition engines are constrained by knock. Knock is an abnormal combustion process that is associated with end-gas autoignition ahead of the propagating flame front, producing rapid pressure oscillations, high local temperature gradients and potential mechanical damage [1–3]. Because knock limits compression ratio, spark timing, boost pressure and load, it also constrains the useful efficiency of spark-ignition engines.

For liquid spark-ignition fuels, knock resistance is commonly expressed through octane number [4]. For gaseous fuels, methane number, *MN*, is the corresponding rating variable.

Methane number expresses the anti-knock quality of a gaseous fuel relative to methane–hydrogen and methane–carbon dioxide reference mixtures [5,6]. However, a fuel-quality number alone is not an engine-design variable. Engine designers also need to know how fuel chemistry modifies the compression ratio that an engine can use without unacceptable knock. For this reason, the present work uses the critical compression ratio measured in a Cooperative Fuel Research engine, denoted $CR_{crit,CFR}$. It is the compression ratio at which a gaseous fuel reaches a prescribed knock threshold in a controlled CFR knock-rating procedure [7]. Thus, *MN* is the fuel-side descriptor of knock resistance, while $CR_{crit,CFR}$ is the machine-side constraint that links fuel chemistry to engine geometry.

The experimental foundation of this work is the CFR-based methane-number and critical-compression-ratio methodology developed for methane, biogas, propane, hydrogen and their blends [7]. In that experimental line, methane number and critical compression ratio were measured for gaseous mixtures in a CFR F-2 engine. These measurements established an empirical relationship between methane number and the critical compression ratio that is accessible before knock.

In this work, CFR denotes the Cooperative Fuel Research engine operated as a gaseous-fuel knock-rating engine in the methane-number procedure [5,7]. Related CFR-engine procedures exist for liquid spark-ignition fuels (octane number) and diesel fuels (cetane number), but the present study uses neither of them and does not use any diesel ignition-quality methodology. Methane number is a knock-resistance descriptor of gaseous fuels for spark-ignition operation, and $CR_{crit,CFR}$ is the compression ratio at which a gaseous fuel reaches the prescribed knock threshold in that procedure. It is therefore a compression-access variable for spark-ignition engines, not an ignition-delay or cetane-type quantity.

This transformation is the key bridge used here. The $MN \rightarrow CR_{crit,CFR}$ relationship allows fuel knock resistance to be inserted into an Otto-cycle reference. Methane number determines the knock-accessible compression ratio, and the Otto-cycle equation determines the corresponding reference efficiency. This provides a reproducible thermodynamic yardstick against which real spark-ignition generator performance can be compared.

This viewpoint is especially relevant for renewable gaseous fuels. Biogas can appear to be a low-quality fuel if judged only by its lower heating value because carbon dioxide dilution reduces volumetric energy content. However, carbon dioxide also increases knock resistance and can allow a higher compression ratio. Hydrogen enrichment can improve flame propagation and combustion stability while modifying knock margin [8,9]. Propane addition increases energy density but reduces knock resistance. More generally, natural-gas composition changes both combustion and knock behavior [10], and the thermodynamic trajectory of the end gas and the fuel chemistry jointly set how far the compression ratio can be raised before knock appears [11]. Therefore, gaseous-fuel performance cannot be assessed from lower heating value alone. It requires a coupled framework linking fuel composition, knock resistance, accessible compression ratio, combustion properties, thermodynamic response and platform-level realization. Such a framework is also useful for interpreting why two fuels with similar heating values may lead to different knock-limited operating windows or two fuels with similar methane numbers may differ in the fraction of the ideal opportunity that a given engine platform realizes.

The need for fuel-aware engine operation adds a further motivation. Renewable and alternative gaseous fuels such as biogas, biomethane, hydrogen-enriched natural gas and propane-containing blends differ in methane number, dilution, flame speed and energy density, so a fixed engine calibration cannot realize the same fraction of the knock-limited opportunity with all of them. Future spark-ignition engines intended for variable renewable gases may therefore need to adapt compression ratio, spark timing, injection strategy, equivalence ratio, exhaust gas recirculation (EGR), boost and valve

timing to the actual fuel quality automatically. Variable displacement and compression ratio [12], EGR [13], pressure-based knock detection [14] and advanced combustion concepts such as homogeneous charge compression ignition (HCCI) [15] and reactivity-controlled compression ignition (RCCI) [16] have been investigated as routes to extend efficient operation across fuels of different reactivity, and an analogous fuel-property and engine-adaptation problem exists in multifuel compression-ignition systems [17]. In this context methane number remains a useful fuel-side descriptor, but it does not quantify how much of the knock-limited opportunity a given engine realizes. That gap is addressed here.

1.2. Historical Origin of X_{fMN}

Previous phenomenological studies proposed that gaseous-fuel quality in spark-ignition engines should not be evaluated from a single property. Fuel behavior depends on methane number, laminar flame speed, energy density, adiabatic flame temperature, hydrogen-to-carbon ratio and specific-heat ratio [18,19].

The historical X_{fMN} formulation attempted to combine several of these descriptors into a methane-normalized multiplicative factor:

$$\bar{X}_{fMN} = \left(\frac{ED^{\circ}_{CH_4}}{ED^{\circ}_{f}}\right)\left(\frac{S^{\circ}_{L,CH_4}}{S^{\circ}_{L,f}}\right)^{0.262}\left(\frac{T^{\circ}_{ad,CH_4}}{T^{\circ}_{ad,f}}\right)^{0.368}\left(\frac{(H/C)_{CH_4}}{(H/C)_{f}}\right)^{0.001}\left(\frac{\gamma^{\circ}_{CH_4}}{\gamma^{\circ}_{f}}\right)^{0.001}. \quad (1)$$

This historical expression did not include an explicit methane-number multiplier [19,20]. Its main structural limitation is that all normalized property ratios equal one for methane. Therefore, any multiplicative expression without a free intercept imposes:

$$\bar{X}_{fMN,CH_4} = 1. \quad (2)$$

When X_{fMN} is reinterpreted as the ratio between measured electrical efficiency and a knock-limited Otto reference, methane gives:

$$X^{\exp}_{fMN,CH_4} = \frac{0.3020}{0.5547} = 0.544. \quad (3)$$

Thus, the historical formulation forces unity on the reference fuel, while the measured realization ratio is approximately 0.544. This is an algebraic anchoring problem. The present work corrects this limitation by introducing a free intercept K and redefining X_{fMN} as a local fuel–engine realization ratio. In this revised interpretation, methane remains a useful reference fuel, but it is no longer forced to represent full realization of the knock-limited thermodynamic opportunity.

The knock-limited Otto reference used in this paper is not introduced without precedent. The MN–$CR_{crit,CFR}$ chain and the corresponding Otto-reference structure were previously reported in the 2024 Energy Conversion and Management article (ECM 2024) [20], and the sensitivity derivatives of the Otto reference with respect to MN, γ° and H/C were subsequently derived in the 2025 Applied Thermal Engineering article (ATE 2025) [21]. The present work does not claim those equations as new. Its contribution is to use that reference as the denominator of a measured BSI/Otto realization ratio and audit the resulting model for identifiability, null-model performance and applicability domain.

1.3. Research Gap, Objective and Hypotheses

The previous X_{fMN} formulation had not been formally audited as a statistical model. Its methane-reference anchoring, denominator-driven behavior, descriptor identifiability and applicability domain had not been quantified. A model with several correlated descriptors calibrated on nine fuels can produce high in-sample agreement without predictive stability.

Likewise, a ratio that is built on a strongly varying denominator can appear to be successful even when most variation comes from the reference.

The research question is: can X_{fMN}, originally proposed as a methane-normalized gaseous-fuel factor, be reformulated as a statistically identifiable realization diagnostic using the $MN \rightarrow CR_{crit,CFR}$ transformation as the physical change of variable between fuel knock resistance and compression accessibility?

The general objective is to reformulate, recalibrate and delimit X_{fMN} for gaseous fuels in spark-ignition engines so that the resulting model is algebraically consistent, physically interpretable, statistically identifiable and explicitly domain-aware.

The hypotheses are:

H1. *The historical methane-normalized model is algebraically anchored and requires a free intercept because* $X_{fMN,CH_4}^{\exp} \neq 1$.

H2. *After MN is used, through* $CR_{crit,CFR}(MN)$*, to construct the knock-limited Otto reference, the residual realization signal is better represented by a reduced model based on* $(H/C)_r$ *and* γ_r *than a full collinear model.*

H3. *Under the nominal MN assignment used in the source series, the reduced model improves measured electrical efficiency prediction relative to a leave-one-out null model. This hypothesis is evaluated as conditional because five engine blends have alternative MN assignments when matched to the thesis database by composition.*

H4. *The reduced model has a limited applicability domain, so predictions outside the convex hull should be reported as unsupported extrapolations rather than validated estimates.*

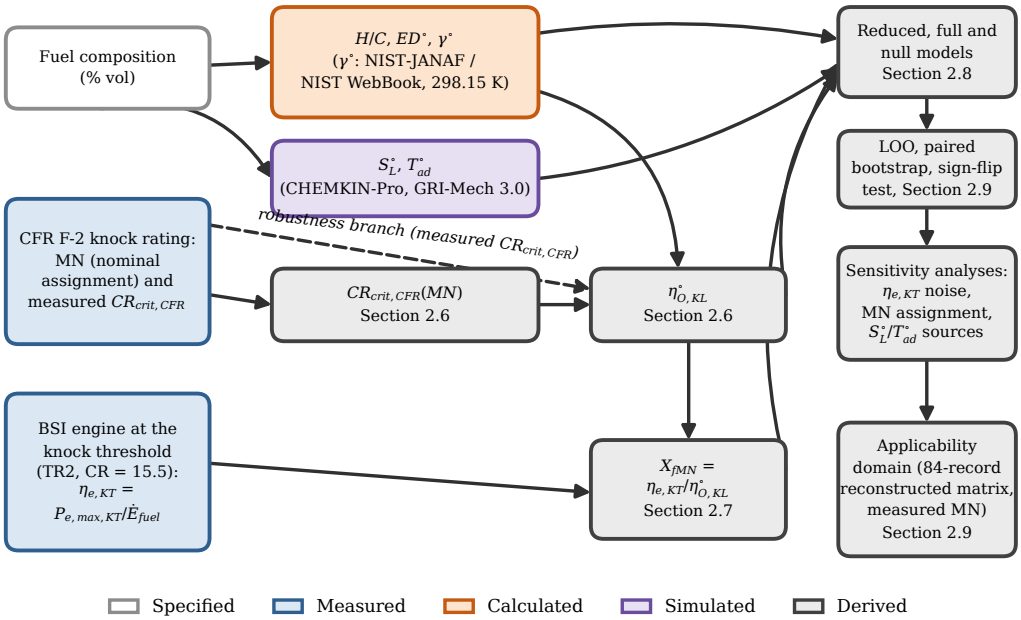
2. Materials and Methods

2.1. Workflow Overview

This work introduces no new experiments. It reanalyzes previously published CFR methane-number and critical-compression-ratio measurements [5,7], biogas spark-ignition (BSI) measurements [9,22–24], the ECM 2024 descriptor and reference formulation [20] and a reconstructed gaseous-fuel property matrix. ATE 2025 [21] is retained as a technical antecedent for the Otto-reference sensitivity expressions and the $MN \rightarrow CR_{crit,CFR} \rightarrow \eta_{Otto}$ chain, not a source of new BSI measurements.

The workflow therefore separates three layers that were previously combined: the fuel-rating layer, represented by MN and $CR_{crit,CFR}$; the ideal-reference layer, represented by the knock-limited Otto efficiency; and the platform-realization layer, represented by measured electrical efficiency at the knock threshold.

All the efficiencies, realization factors, compression ratios, methane numbers, methane-normalized descriptor ratios, regression metrics and applicability-domain diagnostics are dimensionless unless otherwise stated. Quantities are expressed in SI units (MJ m^{-3}, m s^{-1}, K, and kPa) except that engine speed is given in rpm (min^{-1}) and engine displacement in cm^3 (10^{-6} m^3) following common engine practice. The ratios ED_r°, $S_{L,r}^{\circ}$, $T_{ad,r}^{\circ}$, $(H/C)_r$ and γ_r are the methane-to-fuel ratios of each descriptor, defined in Section 2.8, and are therefore dimensionless. Scheme 1 summarizes the workflow.



Scheme 1. Workflow of the revised realization-factor analysis. Fuel composition provides the basis for H/C, ED°, γ°, S_L° and T_{ad}°. γ° is computed from NIST-JANAF/NIST Chemistry WebBook data at 298.15 K [25,26]. S_L° is taken from ECM 2024 for the calibration set, while T_{ad}° is taken from thesis CHEMKIN-PRO equilibrium outputs. CFR knock rating provides MN and $CR_{crit,CFR}$. MN defines $CR_{crit,CFR}(MN)$, and $CR_{crit,CFR}$ with γ° defines the knock-limited Otto reference. BSI engine measurements provide $\eta_{e,KT}$. Their ratio defines X_{fMN}. Full, reduced and null models are audited using leave-one-out, bootstrap and sign-flip tests. The reconstructed 84-record matrix is used only for applicability-domain screening and conditional projections. The predicted MN field from the thesis workflow is retained only as an internal control/provenance field.

2.2. Experimental and Data Provenance

The experimental foundation is the CFR methane-number and critical-compression-ratio methodology used for gaseous-fuel knock rating. In that methodology, methane number and critical compression ratio were measured for gaseous blends in a CFR F-2 engine (Colorado State University, Fort Collins, CO, USA) [7]. The CFR procedure provided both MN and $CR_{crit,CFR}$.

The BSI calibration data come from high-compression spark-ignition engine studies using a Lister Petter TR2 platform (Lister Petter Power Systems Limited, Gloucester, UK) converted to gaseous-fuel spark-ignition operation [9,22–24]. The engine had two cylinders, 1550 cm^3, operated near 1800 rpm, and is treated here according to the BSI calibration series with $CR = 15.5{:}1$. The platform was coupled to an asynchronous generator and an electrical resistance load bank.

The instrumentation of the source campaign included ABB variable-area rotameters, a Piezo-Metrics, Simi Valley, CA, USA, an orifice plate with a U-tube manometer and a Siemens air-pressure transducer (Siemens, Munich, Germany), a SICK MAIHAK S710 gas analyzer (SICK AG, Waldkirch, Germany) and Thermo Scientific 42i-HL gas analyzers (Thermo Fisher Scientific Inc., Franklin, MA, USA), a Kistler 6125C in-cylinder pressure sensor (Kistler Group, Winterthur, Switzerland), a Kistler 4005A intake-pressure sensor (Kistler Group, Winterthur, Switzerland), a Kistler 2614B4 crank-angle encoder and a Kistler KiBox To Go 2893A combustion-analysis system (Kistler Group, Winterthur, Switzerland) system [22]. Electrical power was measured at the generator terminals with a power meter and a power variator; the model and accuracy of these devices are not specified in the source publications and are therefore not propagated into the efficiency uncertainty.

In the primary Energy 2018 source, knock is quantified by the knock peak pressure, KPP, and the BSI knock-threshold operation corresponds to $KPP = 30$–50 kPa (0.3–0.5 bar in the source) over 200 cycles [22]. COV_{IMEP}, the coefficient of variation of the indicated mean effective pressure, is reported only as a stability indicator. The source campaign reports $COV_{IMEP} = 1.98\%$ under negligible knock and $COV_{IMEP} = 3.10\%$ under low knock and notes that values below 5% are expected in normal spark-ignition operation [22]. Pressure-based knock-intensity indicators of this kind have a long history in knock research [14,27].

The 84-record matrix was reconstructed from the thesis-stage database. It includes source blocks, fuel compositions, measured *MN* fields, predicted *MN* control fields and CHEMKIN-PRO outputs. The source blocks include producer-gas blends [28], natural-gas compositions [29], Colorado State University (CSU) knock-rating studies [5,30,31] and Gómez Montoya–Olsen blends [7]. The matrix is used only for applicability-domain screening and conditional projections, not calibration or external validation of $\eta_{e,KT}$.

The reconstruction identified a heat-capacity formula error in the thesis-stage extended matrix. The C_v contributions of C_3H_8 and C_4H_{10} had been interchanged, which understated γ° in propane-containing records. This correction affects the extended matrix only; the nine-fuel calibration γ° values were recalculated independently on the NIST-JANAF/NIST Chemistry WebBook basis [25,26].

Table 1 maps each data component to its source and technical role, and Table 2 summarizes the engines, instruments, software and reproducibility settings. The nine calibration fuels were selected because they have both CFR methane-number information and measured BSI electrical efficiency at the knock threshold. The 84-record matrix has no measured BSI efficiency and was not used for calibration. Author-related references are cited in this paper only where they provide data, equations, experimental procedures or essential methodological background, as identified in Table 1; general statements are supported by independent studies.

Table 1. Data provenance and technical role of each data component.

Data Component	Source	Role in This Work
Methane number, *MN*, of the nine calibration fuels	CFR knock rating of CFR-matched blends [7]; nominal values of the BSI series (Section 2.3)	Input to $CR_{crit,CFR}(MN)$ and the knock-limited Otto reference
Critical compression ratio, $CR_{crit,CFR}$	Measured in the CFR engine for the nine fuels [7]; correlation $CR_{crit,CFR} = 7.1635\exp(0.0069\,MN)$ [20,21] (Section 2.6)	Correlation branch in the main model; measured values only in a sensitivity check
Sensitivity expressions of the reference	ATE 2025 [21]; derivatives of the Otto-reference chain with respect to *MN* and γ°, evaluated in Section 2.6	Local sensitivity analysis of the reference (Section 2.6)
Measured electrical efficiency, $\eta_{e,KT}$	BSI engine campaigns [9,22–24]; maximum electrical power compiled in ECM 2024 [20]; fuel power from Part 2 [19]	Calibration target of X_{fMN}
Fuel composition of the calibration fuels	Engine blend labels of the BSI series (ECM 2024) [20]	Basis of H/C, γ° and ED°
γ°	Computed here from mole-fraction-averaged ideal-gas heat capacities at 298.15 K: NIST-JANAF [25] (CH_4, CO_2, H_2) and NIST Chemistry WebBook [26] (C_3H_8)	Knock-limited Otto reference; reduced model
H/C	Computed from composition; carbon of CO_2 included	Reduced model

Table 1. *Cont.*

Data Component	Source	Role in This Work
ED°, S_L°	ECM 2024 [20] (CHEMKIN-Pro, GRI-Mech 3.0, 101.325 kPa for S_L°)	Full-model audit only
T_{ad}°	Thesis CHEMKIN-PRO equilibrium runs; cross-check with Cantera/GRI-Mech 3.0 [32,33]	Full-model audit only
Original $\bar{X}_{fMN}$ equation	Previous formulation by the authors [18–20]	Equation audited and reformulated
84-record matrix	Reconstructed from the thesis-stage database. Source blocks: producer-gas blends [28] (records 1–35), natural-gas compositions [29] (36–47), producer-gas knock rating [30] (53–67), other CSU knock-rating studies [5,31], and CFR blends [7] (83–103) [a]	Applicability-domain screening and conditional projections only
Predicted *MN* (AVL METHANE 3.0)	Thesis-stage database	Not used in any calculation; retained as a provenance and control field

[a] Record numbers are those of the thesis-stage database (Supplementary Workbook, sheet Matrix84_Provenance); they are not consecutive indices of the 84-record matrix.

Table 2. Experimental platforms, instruments, software and reproducibility settings.

Category	Item	Description
Knock-rating engine	CFR	Cooperative Fuel Research F-2 engine operated on gaseous fuels in the methane-number procedure; provides *MN* and $CR_{crit,CFR}$ [5,7]
BSI engine	Platform	Lister Petter TR2, diesel engine converted to spark-ignition; four-stroke, two cylinders, 1550 cm^3, bore × stroke 98 mm × 101 mm, about 1800 rpm [22]
	Compression ratio	15.5:1 in the BSI calibration series; the engine-specification table of [22] lists 15.1:1. The value 15.5:1 is used only to mark the *MN* at which $CR_{crit,CFR}$ equals the engine compression ratio (Figure 1)
	Load and power	Asynchronous generator and electrical resistance load bank [22]; power meter and power variator at the generator terminals; model and accuracy not reported in the source publications
	Knock threshold	KPP = 30–50 kPa averaged over 200 cycles; maximum electrical power at this threshold [22]
	Combustion stability	COV_{IMEP} = 1.98% (negligible knock) and 3.10% (low knock) [22]
Instruments [22]	Flows	ABB variable-area rotameters (resolution about 1%); Piezo-Metrics Coriolis fuel-mass-flow meter; orifice plate for air with U-tube manometer and Siemens pressure transducer
	Gas analysis	SICK AG, Waldkirch, Germany; Thermo Fisher Scientific Inc., Franklin, MA, USA
	Combustion analysis	Kistler 6125C in-cylinder pressure sensor, Kistler Group, Winterthur, Switzerland; Kistler 4005A intake-pressure sensor, Kistler Group, Winterthur, Switzerland; Kistler 2614B4 crank-angle encoder, Kistler Group, Winterthur, Switzerland (0.1° CA); KiBox To Go 2893A combustion-analysis system, Kistler Group, Winterthur, Switzerland
Thermochemical software	CHEMKIN-PRO, Cantera, AVL METHANE v 12.0	CHEMKIN-PRO (ANSYS, Inc., Canonsburg, PA, USA) with the GRI-Mech 3.0 mechanism (commercial; thesis-stage equilibrium runs, version not recorded); Cantera 3.2.0 with the GRI-Mech 3.0 mechanism, Cantera Developers, Chicago, IL, USA (open source) for the cross-check [32,33]; AVL METHANE 3.0 (AVL List GmbH, Graz, Austria; commercial software), used only for the predicted-*MN* control field
Statistical software	Python v 3.12	Python 3.12.3 with NumPy 2.4.4, SciPy 1.17.1, pandas 3.0.2, Shapely 2.1.2 and Matplotlib 3.10.8 (open source). Calculation and figure scripts and workbooks are provided as Supplementary Materials
Reproducibility	Settings	Paired bootstrap with B = 10,000 and seed 20260930; exact sign-flip test over 2^9 assignments; Gaussian-noise sensitivity with 4000 replicates per level (seed 20260930 plus level index); descriptors at 298.15 K and 101.325 kPa

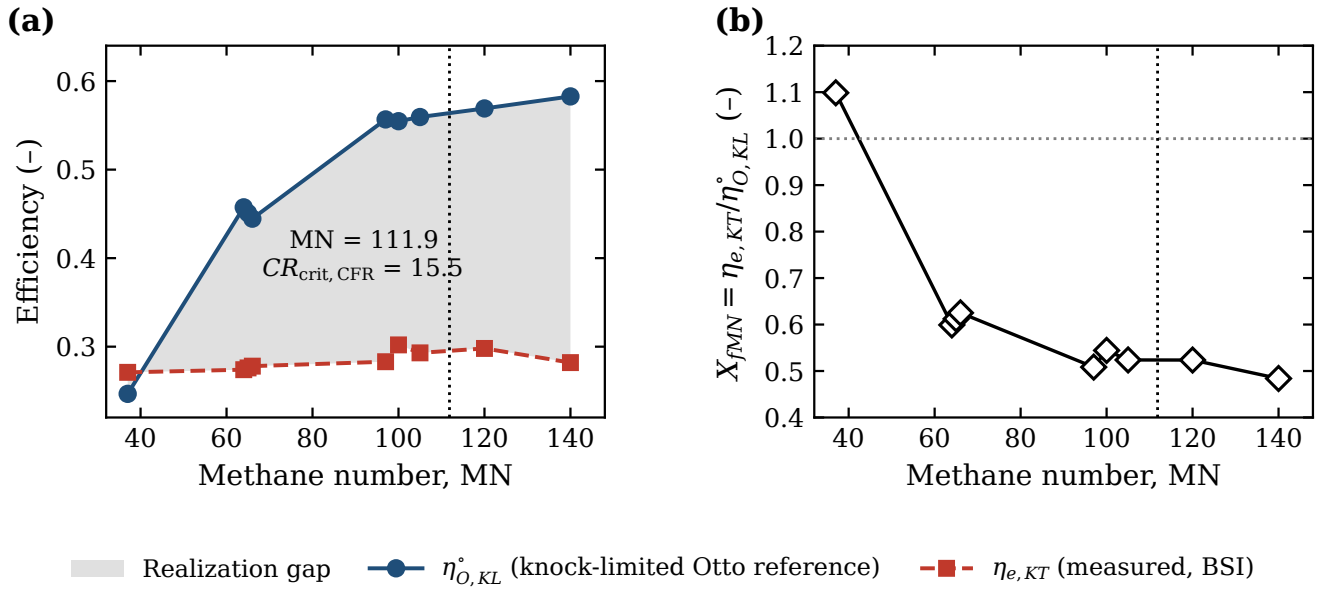


Figure 1. Knock-limited Otto reference and measured electrical efficiency versus methane number: (**a**) $\eta^{\circ}_{O,KL}$ and $\eta_{e,KT}$, with the realization gap shaded and the vertical line at $MN = 111.9$, where $CR_{crit,CFR} = 15.5$; (**b**) X_{fMN}.

2.3. Calibration Set

Table 3 gives the composition and reference-condition descriptors of the nine calibration fuels, and Table 4 summarizes their nominal *MN*, measured electrical efficiency, knock-limited reference and realization ratio under the nominal *MN* assignment used in the source series.

Table 3. Calibration fuels: composition (% by volume), nominal methane number and reference-condition descriptors.

Fuel	*MN* [a]	CH_4 (%)	CO_2 (%)	H_2 (%)	C_3H_8 (%)	ED° [b] (MJ m^{-3})	S_L° [c] (m s^{-1})	T_{ad}° [d] (K)	γ° [e]	H/C [f]
Biogas 60/40	140	60.0	40.0	0	0	3.56	0.2357	2103.4	1.2978	2.40
Biogas 80/20	120	80.0	20.0	0	0	3.57	0.3022	2176.5	1.3010	3.20
57bg + 38CH_4 + 5H_2	105	72.2	22.8	5.0	0	3.58	0.3032	2167.7	1.3043	3.15
100% CH_4	100	100.0	0	0	0	3.58	0.3498	2223.9	1.3043	4.00
54bg + 36CH_4 + 10H_2	97	68.4	21.6	10.0	0	3.59	0.3174	2171.2	1.3083	3.26
83bg + 17C_3H_8	66	49.8	33.2	0	17.0	3.64	0.3283	2176.1	1.2426	2.50
79bg + 16C_3H_8 + 5H_2	65	47.4	31.6	5.0	16.0	3.65	0.3391	2177.1	1.2480	2.58
75bg + 15C_3H_8 + 10H_2	64	45.0	30.0	10.0	15.0	3.66	0.3495	2180.8	1.2536	2.67
100% C_3H_8	37	0	0	0	100.0	3.73	0.4350	2264.9	1.1274	2.67

bg = biogas (60% CH_4 + 40% CO_2, v/v). ED°, S_L° and T_{ad}° refer to stoichiometric fuel–air mixtures at 298.15 K and 101.325 kPa; γ° refers to the unburned fuel gas. [a] Nominal *MN* of the CFR-matched blends [7]. For *MN* 105, 97, 66, 65 and 64 the CFR mixtures differ in composition from the engine blends listed here (Section 2.3). [b] Lower heating value per stoichiometric air requirement, ECM 2024 [20]; the reference state of the volumetric heating value is not documented in the source. [c] CHEMKIN-Pro with GRI-Mech 3.0 at 101.325 kPa [20]; converted from the cm s^{-1} values of the source. [d] Thesis CHEMKIN-PRO equilibrium runs at constant enthalpy and pressure; they agree within 3 K with an independent Cantera/GRI-Mech 3.0 calculation [32,33]. [e] C_p/C_v of the unburned fuel gas as an ideal gas at 298.15 K from mole-fraction-averaged molar heat capacities (NIST-JANAF [25] for CH_4, CO_2 and H_2; NIST Chemistry WebBook [26] for C_3H_8); not the value of the fuel–air mixture. [f] Atomic hydrogen-to-carbon ratio of the complete fuel gas; the carbon of CO_2 is included.

Table 4. Calibration fuels under the nominal *MN* assignment.

Fuel	Nominal MN	$\eta_{e,KT}$	$\eta^{\circ}_{O,KL}$	X_{fMN}
Biogas 60/40	140	0.2820	0.5827	0.4839
Biogas 80/20	120	0.2980	0.5691	0.5236
57bg + 38CH_4 + 5H_2	105	0.2930	0.5594	0.5238
100% CH_4	100	0.3020	0.5547	0.5443
54bg + 36CH_4 + 10H_2	97	0.2830	0.5567	0.5084
83bg + 17C_3H_8	66	0.2780	0.4446	0.6251
79bg + 16C_3H_8 + 5H_2	65	0.2760	0.4509	0.6122
75bg + 15C_3H_8 + 10H_2	64	0.2740	0.4574	0.5991
100% C_3H_8	37	0.2710	0.2467	1.0986

The measured electrical efficiency range is

$$0.2710 \leq \eta_{e,KT} \leq 0.3020. \tag{4}$$

The knock-limited Otto reference range is

$$0.2467 \leq \eta^{\circ}_{O,KL} \leq 0.5827. \tag{5}$$

Thus, the reference varies much more strongly than the measured electrical efficiency.

The nominal *MN* values of five engine blends, 105, 97, 66, 65 and 64, correspond to CFR mixtures of different compositions. Assigning the *MN* values that are listed in the thesis database to engine blends based on their own compositions removes the advantage of the reduced model over the null model. Therefore, the nominal *MN* assignment is treated as a source-series convention and explicitly declared as a limitation.

2.4. Thermochemical Descriptors

The descriptors included in the historical full model represent different physical layers of gaseous-fuel combustion. ED° represents energy supplied per stoichiometric air requirement. S°_L is associated with flame propagation. T°_{ad} is linked to thermal intensity and end-gas temperature. H/C summarizes the elemental composition of the complete fuel blend, including carbon in CO_2. γ° controls the ideal Otto-cycle response and reflects differences in thermodynamic mixture behavior.

For the adopted full-model audit, S°_L is taken from ECM 2024 [20], and T°_{ad} is taken from thesis CHEMKIN-PRO equilibrium outputs. These outputs give T°_{ad} = 2223.85 K for methane and 2180.82 K for the *MN* 64 blend in agreement with the independent Cantera/GRI-Mech 3.0 cross-check within 3 K [32,33]. Therefore, these values were adopted for the final full-model audit, while S°_L was retained from ECM 2024.

2.5. Measured Electrical Efficiency

The fuel energy input rate, written with the lower heating value (LHV) of the fuel, is

$$\dot{E}_{fuel,f} = \dot{m}_f \, LHV_{m,f}, \tag{6}$$

or, equivalently,

$$\dot{E}_{fuel,f} = \dot{V}_f \, LHV_{v,f}. \tag{7}$$

The measured electrical efficiency at the knock threshold is

$$\eta_{e,KT,f} = \frac{P_{e,\max,KT,f}}{\dot{E}_{fuel,f}}. \tag{8}$$

This is an electrical generator-set efficiency. It includes combustion, thermodynamic conversion, mechanical losses, generator efficiency, accessories and operating strategy. Therefore,

$$\eta_{e,KT} \neq \eta_{Otto}. \tag{9}$$

This distinction is central: X_{fMN} is not a pure thermodynamic irreversibility factor but a platform-level realization factor.

2.6. Knock-Limited Otto Reference

The ideal Otto efficiency is

$$\eta_{Otto} = 1 - \frac{1}{CR^{\gamma-1}}. \tag{10}$$

For a knock-limited gaseous fuel, the accessible compression ratio is constrained by $CR_{crit,CFR}$. Therefore, the knock-limited Otto reference is

$$\eta^{\circ}_{O,KL,f} = 1 - CR^{-(\gamma^{\circ}_{f}-1)}_{crit,CFR,f}. \tag{11}$$

The standardized correlation branch uses

$$CR_{crit,CFR,f} = 7.1635\, e^{0.0069\, MN_f}. \tag{12}$$

This correlation was reported in ECM 2024 [20] and used as part of the Otto-reference chain further analyzed in ATE 2025 [21]. This equation transforms the fuel-side knock-resistance descriptor MN into the machine-side compression constraint $CR_{crit,CFR}$, which then determines the knock-limited Otto reference. The correlation branch is retained because it provides a smooth and homogeneous reference that is applicable both to the nine calibration fuels and the 84-record projection matrix, where measured $CR_{crit,CFR}$ values are unavailable.

The local sensitivities of the reference, consistent with the previously reported derivatives for the Otto-reference chain [21], are

$$\frac{\partial \eta^{\circ}_{O,KL}}{\partial MN} = 0.0069(\gamma^{\circ} - 1)CR^{-(\gamma^{\circ}-1)}_{crit,CFR} \tag{13}$$

and

$$\frac{\partial \eta^{\circ}_{O,KL}}{\partial \gamma^{\circ}} = \ln\left(CR_{crit,CFR}\right)CR^{-(\gamma^{\circ}-1)}_{crit,CFR} = (1.9690 + 0.0069\, MN)CR^{-(\gamma^{\circ}-1)}_{crit,CFR}. \tag{14}$$

At $MN = 100$ and $\gamma^{\circ} = 1.30$, the magnitude of the MN derivative is approximately 9×10^{-4} per MN unit, whereas the derivative with respect to γ° is approximately 1.2 per unit γ°. MN is essential because it defines the knock-accessible compression reference, but the local differential response of the Otto reference is much stronger with respect to γ°.

2.7. Redefinition of X_{fMN}

The maximum electrical output at the knock threshold can be written as

$$P_{e,\max,KT,f} = X_{fMN}(f)\, \dot{E}_{fuel,f}\, \eta^{\circ}_{O,KL,f}. \tag{15}$$

Therefore,

$$X_{fMN}(f) = \frac{P_{e,\max,KT,f}}{\dot{E}_{fuel,f}\, \eta^{\circ}_{O,KL,f}} = \frac{\eta_{e,KT,f}}{\eta^{\circ}_{O,KL,f}}. \tag{16}$$

This redefines X_{fMN} as a BSI/Otto realization factor. Since X_{fMN} is a ratio between an electrical generator-set efficiency and a constructed ideal reference, it is not itself an efficiency. Therefore, $X_{fMN} > 1$ is not thermodynamically forbidden.

2.8. Full, Reduced and Null Models

The corrected full model is

$$X_{fMN} = K\, ED_r^a\, S_{L,r}^b\, T_{ad,r}^c\, (H/C)_r^d\, \gamma_r^e, \tag{17}$$

where each descriptor is normalized relative to methane. As in Equation (1), each normalized descriptor is the methane-to-fuel ratio,

$$(H/C)_r = \frac{(H/C)_{CH_4}}{(H/C)_f}, \qquad \gamma_r = \frac{\gamma^\circ_{CH_4}}{\gamma^\circ_f}, \tag{18}$$

and likewise for ED_r, $S_{L,r}$ and $T_{ad,r}$. A fuel with a lower specific-heat ratio than methane therefore has $\gamma_r > 1$, and a positive exponent e means that X_{fMN} increases as γ°_f decreases.

The reduced model is

$$X_{fMN} = K\, (H/C)_r^d\, \gamma_r^e. \tag{19}$$

This reduced form does not imply that ED°, S_L° or T_{ad}° are physically irrelevant. It means that they are not separately identifiable as independent exponents in the present nine-fuel BSI calibration set.

Because X_{fMN} is defined as a ratio, it may inherit much of its variance from the denominator. Therefore, a leave-one-out null model was defined,

$$\eta^{null}_{e,KT,f} = \bar{\eta}_{e,KT,-f}, \tag{20}$$

where $\bar{\eta}_{e,KT,-f}$ is the mean measured electrical efficiency of the other eight fuels. The corresponding null realization factor is

$$X^{null}_{fMN,f} = \frac{\bar{\eta}_{e,KT,-f}}{\eta^\circ_{O,KL,f}}. \tag{21}$$

This null model tests whether the reduced model captures residual realization information beyond denominator-induced behavior.

2.9. Applicability Domain and Sensitivity Analyses

The applicability domain is defined in the reduced-model descriptor space:

$$(\ln(H/C)_r,\ \ln\gamma_r). \tag{22}$$

Two criteria are used: a rectangular box, where each predictor lies within the calibration minimum–maximum range, and a convex hull, where the joint point lies inside the polygon spanned by the nine calibration fuels [34,35]. Only the convex hull is treated as strict interpolation. Box-only points are reported separately, and points outside both criteria are classified as unsupported extrapolations.

Two continuous diagnostics complement this classification. The distance to the hull, d_{hull}, is the Euclidean distance in the $(\ln(H/C)_r, \ln\gamma_r)$ plane from a record to the convex hull of the calibration fuels; it is zero for records inside the hull. The leverage of a record is $h = \mathbf{x}^{\mathrm{T}}(\mathbf{X}^{\mathrm{T}}\mathbf{X})^{-1}\mathbf{x}$, where $\mathbf{x} = [1, \ln(H/C)_r, \ln\gamma_r]^{\mathrm{T}}$ and $\mathbf{X}$ is the design matrix of the nine calibration fuels. Records with h above the Williams-type threshold $h^* = 3(p+1)/n = 1.0$, with $p = 2$ predictors and $n = 9$ fuels, are flagged as higher-risk extrapolations [34,35].

Predictive error was quantified by the leave-one-out (LOO) root-mean-square error, RMSE, computed either in X_{fMN} space ($RMSE_{X,LOO}$) or electrical efficiency space ($RMSE_{\eta,LOO}$). The improvement factor is the ratio of the null-model RMSE to the reduced-model $RMSE_{\eta,LOO}$.

The sensitivity analyses included:

1. Leave-one-out refitting;
2. Paired bootstrap with $B = 10{,}000$;
3. Exact sign-flip test over 2^9 assignments;
4. Gaussian noise sensitivity on $\eta_{e,KT}$;
5. Removal of the high-turbulence biogas 60/40 point;
6. Removal of both extreme fuels;
7. Reassignment of MN to five engine blends using composition-consistent thesis values;
8. Measured $CR_{crit,CFR}$ robustness branch.

Collinearity was assessed using variance inflation factors (VIFs) and the condition number [36,37]. The measured $CR_{crit,CFR}$ branch is reported only as a diagnostic sensitivity check and is not adopted as the main model because the final formulation uses the constructed $CR_{crit,CFR}(MN)$ reference consistently across the calibration and domain analyses.

This sequence of tests was designed to distinguish three questions: whether the model fits the calibration data, whether it outperforms a denominator-driven null model, and whether the fitted coefficients remain meaningful when the descriptor source, fuel assignment or calibration geometry is perturbed.

3. Results

3.1. Knock-Limited Reference Versus BSI Realization

Figure 1 compares the knock-limited Otto reference and the measured BSI electrical efficiency. $\eta^{\circ}_{O,KL}$ increases strongly with methane number. For propane, $MN = 37$ and $\eta^{\circ}_{O,KL} = 0.2467$. For biogas 60/40, $MN = 140$ and $\eta^{\circ}_{O,KL} = 0.5827$. In contrast, the measured electrical efficiency remains in a narrow band:

$$0.2710 \leq \eta_{e,KT} \leq 0.3020. \tag{23}$$

This is the experimental origin of the realization-gap concept. The condition $MN = 111.9$ corresponds to $CR_{crit,CFR} = 15.5$, which is the fixed compression ratio used as a reference for the BSI calibration series. Above this value, the fuel has more knock resistance than the fixed-compression engine can exploit geometrically.

For propane, $X_{fMN} = 1.0986$. For methane, $X_{fMN} = 0.5443$. For biogas 60/40, $X_{fMN} = 0.4839$. The propane point exceeds unity. This does not imply efficiency above unity; it means that the constructed knock-limited Otto reference for propane is lower than the measured electrical efficiency of the tested fixed-compression platform.

3.2. Null-Model Benchmark

Under the nominal MN assignment used in the source series, the deterministic leave-one-out errors are

$$RMSE^{null}_{\eta,LOO} = 0.01170, \tag{24}$$

and

$$RMSE^{red}_{\eta,LOO} = 0.00557. \tag{25}$$

The improvement factor is therefore

$$\frac{0.01170}{0.00557} = 2.10. \tag{26}$$

A paired bootstrap over the nine fuels, with $B = 10{,}000$ and seed 20260930, gives a percentile interval of 1.55–3.90. The reduced model has lower absolute error for all nine fuels. An exact sign-flip test over 2^9 possible sign assignments gives $p = 0.0020$, one-sided.

This result is conditional; see Figure 2. Removing the high-turbulence biogas 60/40 point reduces the improvement to 1.27×. Removing both extreme fuels reduces it to 0.77×. Assigning the *MN* values that are listed in the thesis database to five engine blends based on their own compositions reduces the improvement to 0.89×. Therefore, H3 is supported for the deterministic set under the nominal *MN* assignment but not unconditionally confirmed.

Noise sensitivity was evaluated using the closest available repeatability proxy from Energy 2018 [22]. With Gaussian relative noise of $1\sigma = 0.5\%$, used as a conservative proxy for the reported 0.42% relative standard deviation of brake thermal efficiency under negligible knock, the median improvement remains approximately 2.03×, with the reduced model favored in 100% of replicates. With $1\sigma = 1.0\%$, the median improvement is 1.87×, with the reduced model favored in 99.0% of replicates. Treating the 1.94% repeatability value as 1σ is retained only as a conservative stress test; under that assumption, the median improvement ranges from 1.47× to 1.77×, with the reduced model favored in 85–94% of replicates.

These results show that the deterministic advantage over the null model is not merely a consequence of in-sample fitting. However, they also show that the strength of the advantage depends on the fuel-label lineage and the two extreme descriptor-space cases.

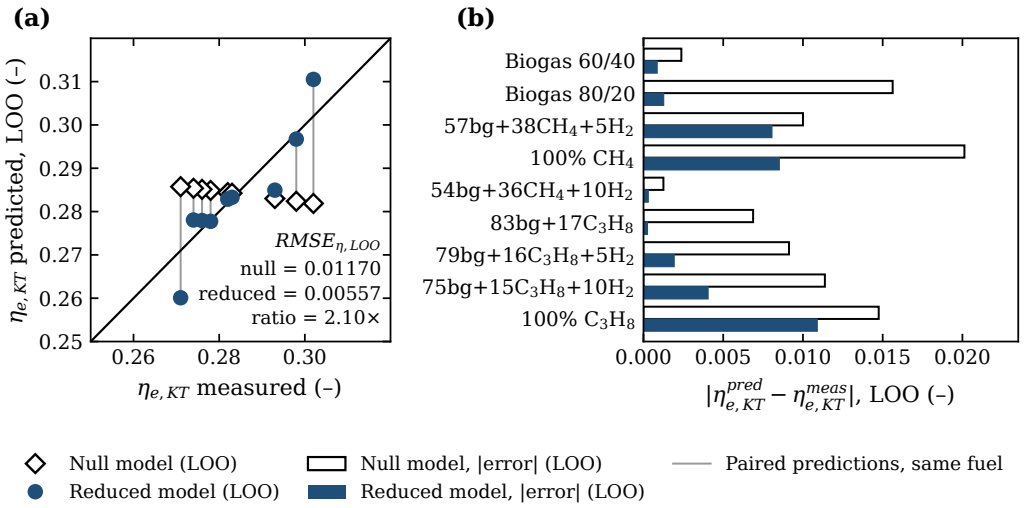


Figure 2. Leave-one-out prediction of electrical efficiency by the null and reduced models under the nominal *MN* assignment used in the source series: (**a**) predicted versus measured values; (**b**) absolute errors by fuel. $RMSE_{\eta,LOO}$: null = 0.01170, reduced = 0.00557.

3.3. Reduced Model Versus Full Model

The final reduced model under the nominal *MN* assignment is

$$X_{fMN} = 0.5506\,(H/C)_r^{-0.3036}\,\gamma_r^{5.5490}. \tag{27}$$

It gives

$$R^2 = 0.9982, \quad R^2_{adj} = 0.9976, \tag{28}$$

$$VIF_{\max} = 1.26, \quad \kappa = 5.25, \tag{29}$$

and

$$RMSE_{X,LOO} = 0.0166. \tag{30}$$

The full model gives

$$RMSE_{X,LOO} = 0.0614. \tag{31}$$

Thus, the full model has approximately 3.7 times the leave-one-out error of the reduced model in X-space; see Figure 3. In electrical efficiency space, the full model gives $RMSE_{\eta,LOO} = 0.01838$, worse than both the null model and the reduced model.

The null hypothesis $K = 1$ is rejected with

$$t = -63.6, \quad p \approx 10^{-9}. \tag{32}$$

Thus, H1 is supported.

The reduced model barely moves when a fuel is removed. The in-sample and leave-one-out values differ by at most 0.039 for propane, 0.009 for methane, and 0.0024 or less for the other seven fuels.

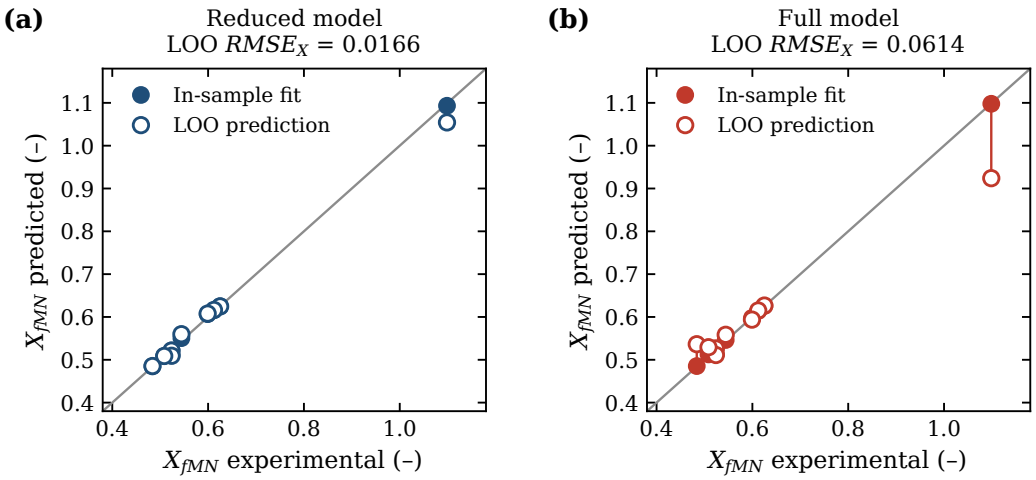


Figure 3. Leave-one-out parity plots in X_{fMN}-space: (**a**) reduced model, $RMSE_{X,LOO} = 0.0166$; (**b**) full model, $RMSE_{X,LOO} = 0.0614$ with S_L° from ECM 2024 and T_{ad}° from thesis CHEMKIN-PRO equilibrium runs. Filled markers: in-sample; open markers: leave-one-out.

3.4. Parameter Identifiability

The full five-descriptor model is not identifiable. In the adopted descriptor set, its VIF values range from 50.1 to 533.1. Across six S_L°/T_{ad}° descriptor sets—the adopted set; ECM 2024 as printed; ECM 2024 with the T_{ad}° values of *MN* 66 and *MN* 65 taken from Part 2; the Part 2 ratios; the thesis CHEMKIN-PRO S_L° and T_{ad}°; and an independent Cantera/GRI-Mech 3.0 calculation—the maximum VIF ranges from 191 to 12,992 and $RMSE_{X,LOO}$ exceeds that of the reduced model in every case. Figure 4 shows the full-model coefficients obtained under five fitting criteria together with the leave-one-out ranges of the full and reduced models.

The measured CR_{crit} branch gives $K = 0.542$, $d = -0.254$, $e = 5.52$ and $RMSE_{\eta,LOO} = 0.00361$. This branch is reported only as a diagnostic sensitivity check and is not adopted as the main model because the final formulation uses the constructed $CR_{crit,CFR}(MN)$ reference consistently across the calibration and domain analyses.

In Figure 4, the full-model exponents a, b and c move by several units from one fitting criterion to another, and their leave-one-out ranges include zero, whereas d and e of the reduced model remain within narrow bands and K stays close to the methane ratio. This is the graphical counterpart of the VIF diagnostics: the exponents of ED°, S_L° and T_{ad}° cannot be identified from nine fuels.

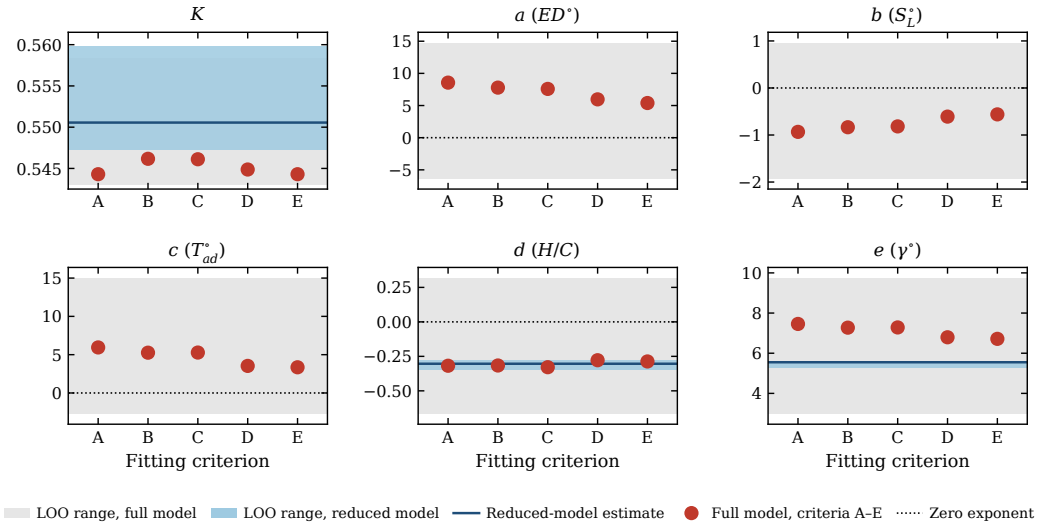


Figure 4. Full-model coefficients under five fitting criteria. A: log-space fit with K fixed at the methane value; B: log-space ordinary least squares (OLS) with free K; C: nonlinear least squares in X_{fMN}; D: Huber iteratively reweighted least squares (IRLS) in log space, $c = 1.345$; E: global L_1-error minimization in X_{fMN}. Gray bands: full-model leave-one-out ranges; blue bands: reduced-model leave-one-out ranges; line: reduced-model estimate.

3.5. Decomposition of the γ_r Exponent and the Reference

The exponent $e = 5.5490$ is physically large and must not be interpreted as the total effect of γ° on engine efficiency. Because

$$X_{fMN} = \frac{\eta_{e,KT}}{\eta^\circ_{O,KL}}, \tag{33}$$

part of the apparent dependence of X_{fMN} on γ_r is induced by the denominator.

An exact decomposition gives

$$e = 5.549 = -0.34\ (\text{realization}) + 5.89\ (\text{reference}). \tag{34}$$

The sign and magnitude of the fitted γ_r exponent are therefore dominated by the constructed reference. Reversing the sign would require methane efficiency to exceed propane efficiency by an unrealistic factor of approximately 2.4.

The range of $\eta^\circ_{O,KL}$ across the calibration set is 0.336, from 0.2467 for propane to 0.5827 for biogas 60/40. Symmetric path decomposition attributes approximately 24% of this range to $CR_{crit,CFR}(MN)$ and 76% to γ°. This does not invalidate the $MN \rightarrow CR_{crit,CFR}$ bridge, but it delimits its numerical weight within this calibration set.

3.6. Applicability Domain

Figure 5 maps the reconstructed 84-record matrix in the reduced-model descriptor space:

$$\ln(H/C)_r \text{ versus } \ln\gamma_r. \tag{35}$$

After correction of the extended-matrix γ° values, the classification is:

$$23 \text{ inside hull}, \quad 3 \text{ box-only}, \quad 58 \text{ outside}. \tag{36}$$

Thus, 58 of 84 records, approximately 69%, remain outside the supported descriptor domain. H4 is therefore supported.

Table 5 reports the continuous diagnostics defined in Section 2.9. All the inside-hull records have $d_{\text{hull}} = 0$ and $h < h^*$, consistent with interpolation. The three box-only records

lie within 0.0046 log units of the hull and none exceeds h^*, so the continuous metrics do not reclassify them as interpolations. Of the 58 outside records, 47 exceed h^*, which confirms that they are extrapolations rather than supported predictions.

Table 5. Applicability-domain diagnostics.

Class	n	Median d_{hull}	Max d_{hull}	Median h	Max h	$h > 1.0$
Inside hull	23	0	0	0.371	0.593	0
Box only	3	0.0002	0.0046	0.273	0.360	0
Outside	58	0.249	1.463	2.305	18.726	47

Of the 23 inside-hull records, eight lie within 0.01 log units of a calibration fuel. Therefore, the interpolation support rests on approximately 15 distinct mixtures. This distinction matters because nominally inside-hull counts can overstate diversity when several records cluster around the same calibration point.

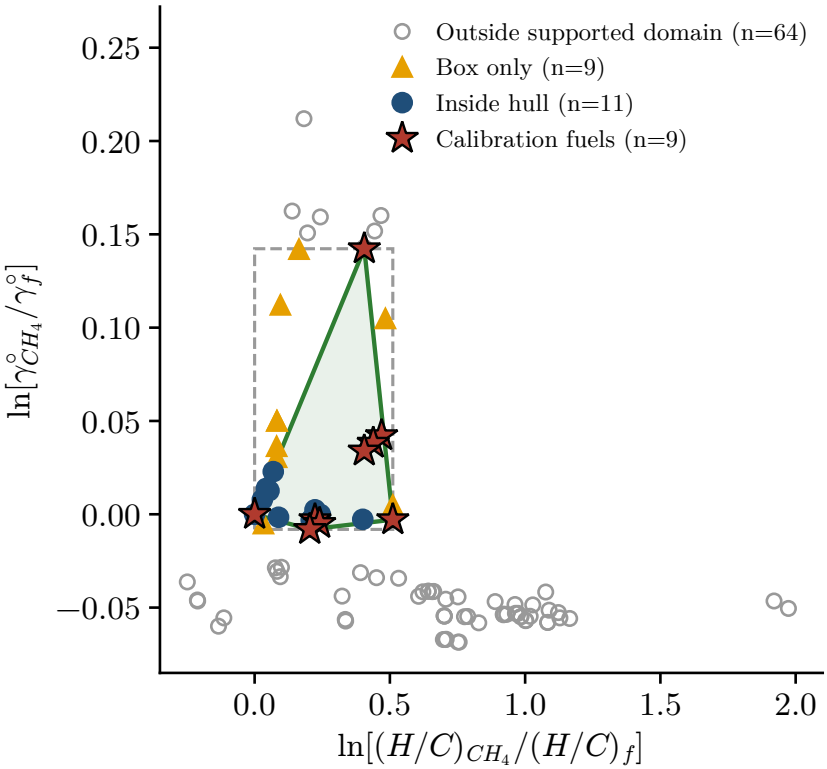


Figure 5. Applicability domain in $\ln(H/C)_r$–$\ln\gamma_r$ space: Full 84-record matrix, with 23 records inside the hull, 3 box-only records, and 58 outside the hull, together with an enlargement of the calibration domain.

3.7. Conditional Efficiency Projections

Figure 6 shows conditional projections of $\eta_{e,KT}$ over the reconstructed 84-record matrix. Inside-hull projected values span approximately

$$0.2825 \leq \hat{\eta}_{e,KT} \leq 0.3055. \tag{37}$$

Box-only projected values span approximately

$$0.2759 \leq \hat{\eta}_{e,KT} \leq 0.2985. \tag{38}$$

The measured BSI calibration range is

$$0.2710 \leq \eta_{e,KT} \leq 0.3020. \tag{39}$$

These are conditional projections, not independent validation data, because measured BSI electrical efficiencies exist only for the nine calibration fuels. The projection bands are therefore useful for screening whether a composition lies in a plausible realization interval but not claiming that the model has been validated on those fuels.

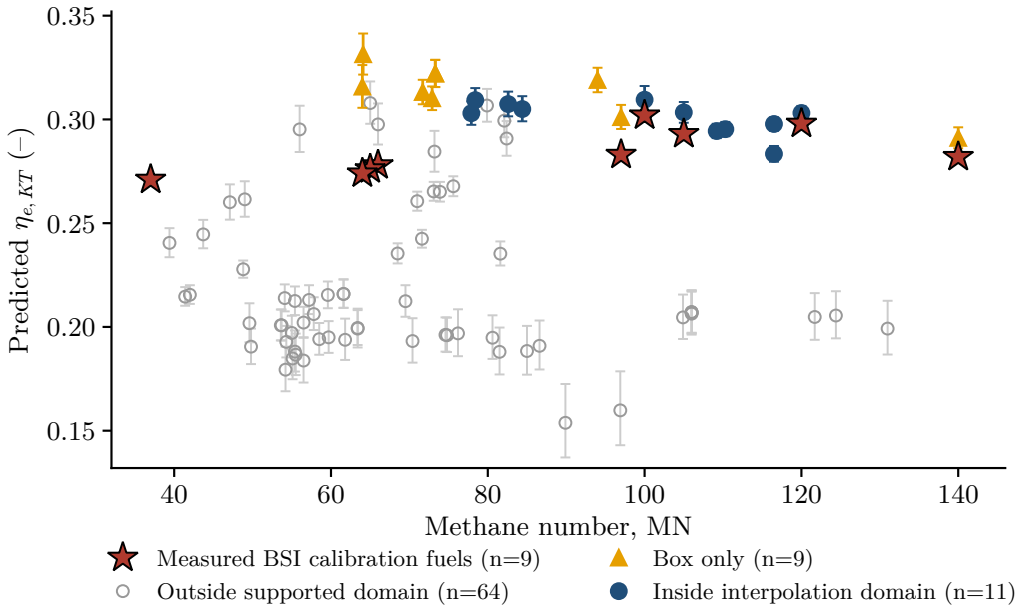


Figure 6. Conditional projections of $\eta_{e,KT}$ over the reconstructed 84-record matrix. Error bars are 95% prediction intervals using Student's t with 6 degrees of freedom, shown only for inside-hull and box-only records. The shaded band is the measured BSI calibration range, 0.2710–0.3020. These projections are not independent validation data.

3.8. Response Surface of the Reduced Model

Figure 7 shows the reduced model, $X_{fMN} = K\,(H/C)_r^d\,\gamma_r^e$, as a surface over the range of the fuel-gas descriptors, $2.4 \le H/C \le 4.0$ and $1.10 \le \gamma^\circ \le 1.33$. Panel (a) gives the surface and panel (b) its plan view with contours together with the nine calibration fuels (labeled by nominal MN) and the convex hull of the calibration set. Regions outside the hull are faded because they are extrapolations.

Within the plotted rectangle the model gives X_{fMN} between 0.42 and 1.42. The surface rises steeply as γ° decreases and only weakly as H/C increases: near $\gamma^\circ = 1.30$, a decrease of 0.01 in γ° raises X_{fMN} by about 4.4%, whereas a 10% increase in H/C raises it by about 2.9%. This asymmetry reflects the exponents, which are dominated by the denominator (Section 3.5).

Eight of the nine calibration fuels lie in a narrow range of γ°, from 1.243 to 1.308, where the model gives X_{fMN} between 0.48 and 0.70 inside the hull (measured ratios 0.484–0.625, Table 4). Propane is isolated at $\gamma^\circ = 1.127$, where $X_{fMN} = 1.09$ (measured 1.0986). The calibration hull is therefore a wedge: a wide upper band, supported by eight fuels, and a lower wedge ($\gamma^\circ < 1.24$), about 40% of the hull area, whose only support is the propane vertex and where the model gives 0.63–1.09.

Values of X_{fMN} above 1 occur over 24.6% of the plotted rectangle, almost entirely toward low γ° and outside the hull. Only 1.8% of that region lies inside the hull in the immediate neighborhood of the propane vertex (γ° below 1.15). Hence values close to or above 1 in Figure 7 are not predictions that are supported by the calibration set: they follow from extending the exponent $e = 5.549$ beyond the observed range of γ°. Propane alone has leverage $h = 0.88$ and contributes 77% of the variance of $\ln X_{fMN}$ in the calibration set.

The surface should therefore be read as a map of where the model is supported (the upper band) and where it depends on a single fuel (the lower wedge), not a fuel ranking.

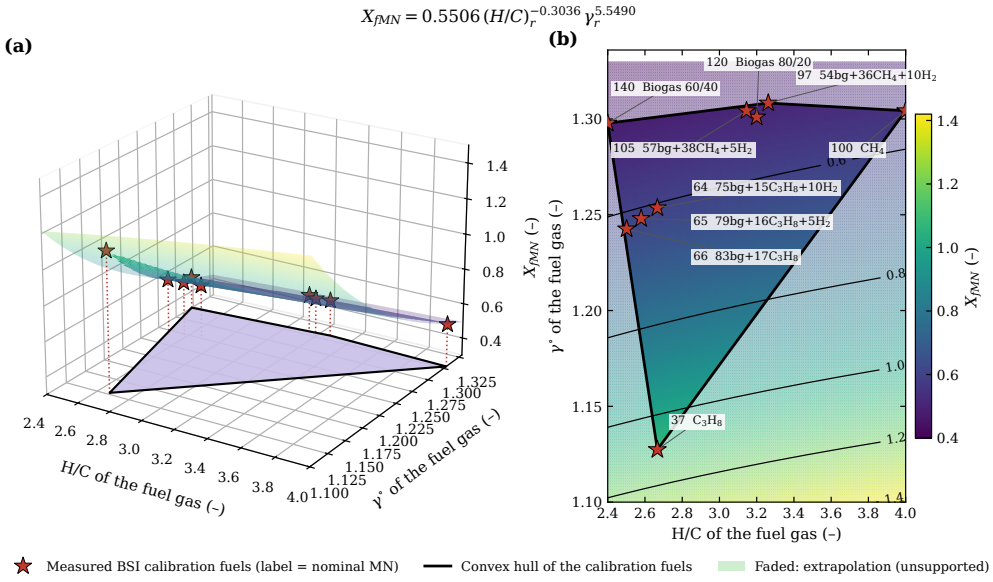


Figure 7. Response surface of the reduced model, $X_{fMN} = 0.5506\,(H/C)_r^{-0.3036}\,\gamma_r^{5.5490}$: (**a**) three-dimensional surface; (**b**) plan view with contours. Stars: the nine calibration fuels, labeled with their nominal *MN*. Solid line: convex hull of the calibration fuels. Faded area: extrapolation outside the hull, not supported by the calibration set.

3.9. MN-Matched Consistency and $CR_{crit,CFR}$ Robustness

A consistency screen was performed using nominally *MN*-matched cases. With the corrected matrix, the errors are:

$$0.34\%, \quad 0.42\%, \quad 1.31\%, \quad 4.91\%. \tag{40}$$

The mean error is 1.75%, and the maximum error is 4.91%. Only *MN* 140 and *MN* 120 compare the same fuel. For *MN* 105 and *MN* 97, the comparison involves CFR records with the same nominal *MN* but different compositions from the BSI engine blends. Therefore, the screen is retained only as a consistency screen by nominal *MN*, not same-fuel validation.

3.10. Summary of Results

The corrected thermochemical basis supports H1, H2 and H4 and conditionally supports H3 under the nominal *MN* assignment used in the source series.

H1. *The free intercept $K = 0.5506$ removes the methane singularity. The measured ratio for methane is 0.544.*

H2. *The reduced model is the identifiable representation. $RMSE_{X,LOO} = 0.0166$ against 0.0614 for the full model.*

H3. *H3 is conditionally supported for the deterministic set under the nominal MN assignment, with improvement* 2.10×*, bootstrap interval 1.55–3.90, nine of nine fuels improved and $p = 0.0020$. Its margin depends on the MN assigned to five engine blends and the extreme fuels.*

H4. *H4 is supported: 58 of 84 records, approximately 69%, lie outside the supported domain. Inside-hull projections reproduce the measured range but remain conditional. The response surface (Figure 7) shows that about 40% of the hull area rests on a single fuel, propane.*

4. Discussion

4.1. What the Regularization Proves

The purpose of this work is not to claim that X_{fMN} is independent of the Otto reference. The diagnostic correlation

$$\mathrm{corr}\left(\ln X_{fMN}, \ln \eta^{\circ}_{O,KL}\right) = -0.993 \tag{41}$$

shows that much of X_{fMN} is inherited from the denominator.

The contribution is to quantify this dependence, benchmark it against a null model and determine whether a statistically identifiable residual realization signal remains. Under the nominal *MN* assignment, the reduced model improves leave-one-out electrical efficiency prediction by 2.10× over the null model. However, this improvement disappears if five engine blends are assigned the *MN* values listed in the thesis database for their own compositions. Therefore, the result must be interpreted as conditional and local.

This distinction avoids two opposite overinterpretations. The model is not merely a restatement of the denominator because it improves the null benchmark under the nominal source-series assignment. But it is also not an unconditional validation because the result depends on fuel-lineage decisions that must be documented when the method is applied to new datasets.

4.2. Physical Interpretation of $K \neq 1$

The free intercept $K = 0.5506$ should be interpreted as a platform-level realization factor for the methane-normalized reference case. For methane,

$$\eta_{e,KT} = 0.3020, \quad \eta^{\circ}_{O,KL} = 0.5547, \tag{42}$$

and therefore

$$X^{\mathrm{exp}}_{fMN,CH_4} = 0.5443. \tag{43}$$

The fitted K is close to this value but estimated from all nine fuels. Therefore, K is not a universal constant and not a pure thermodynamic irreversibility factor. It includes combustion, finite-time operation, mechanical losses, generator efficiency, accessories and operating strategy.

4.3. Why MN Changes Role Rather than Disappears

The revised formulation does not remove *MN*. It assigns *MN* to the reference:

$$MN \rightarrow CR_{crit,CFR}(MN) \rightarrow \eta^{\circ}_{O,KL}. \tag{44}$$

Reintroducing *MN* inside the residual model would duplicate knock-resistance information that was already used to construct the reference. However, because *MN* and γ° are correlated in the calibration set, the separation should be interpreted thermodynamically rather than as statistical orthogonality.

This placement also makes the model easier to adapt. If a future study measures $CR_{crit,CFR}$ directly for each fuel, the reference can be rebuilt with measured critical compression ratios. If only *MN* is available, the correlation branch provides a consistent reference for screening and comparison.

4.4. Why $CR_{crit,CFR}$ Is the Central Bridge

The $CR_{crit,CFR}$ transformation is the conceptual hinge of the paper. Without it, *MN* would remain a fuel-rating number and the Otto-cycle equation would remain a machine equation with an unspecified compression ratio. By using $CR_{crit,CFR}(MN)$, the fuel rating becomes a compression-access variable.

This also explains why high methane number does not automatically produce high measured electrical efficiency in the BSI engine. If the fixed engine compression ratio is below the fuel's critical compression ratio, the fuel contains unused knock margin. In such cases, a low X_{fMN} value does not mean that the fuel is poor; it means that the platform cannot fully exploit the compression ratio that is theoretically enabled by the fuel.

4.5. Why the Full Model Fails

The full model fails not because ED°, S_L° or T_{ad}° are physically meaningless. These variables are important for combustion, flame development, dilution effects, heat release and knock behavior. The full model fails because the nine-fuel calibration set cannot identify their independent exponents under strong collinearity.

The reduced model is therefore not a claim of reduced physics. It is a regularized statistical representation of what the available data can identify.

4.6. Why H/C and γ° Remain in the Reduced Model

The reduced model retains H/C and γ° because they provide the most stable residual representation after MN has been assigned to the knock-limited Otto reference. H/C is compositional. It helps to distinguish methane-rich, propane-containing, hydrogen-enriched and carbon-dioxide-diluted blends after the primary knock-access effect has been assigned to MN. γ° is thermodynamic. It affects the Otto reference directly and also appears as a residual realization descriptor.

The exponent on γ_r must be interpreted cautiously. It is not a universal physical exponent. It combines a reference-induced component and a residual platform-realization component.

4.7. Domain Declaration and Practical Implications

The convex-hull analysis is part of the model. The fact that 58 of 84 records require extrapolation means that unsupported application is not a hypothetical risk but a dominant case in the broader matrix. Thus, X_{fMN} should not be used to rank arbitrary gaseous fuels. It should be used only within the declared interpolation domain or otherwise reported as extrapolative. Figure 7 makes this visible: the supported domain is a wedge whose upper band is anchored by eight fuels with γ° between 1.243 and 1.308, whereas its lower wedge, where the model approaches or exceeds $X_{fMN} = 1$, is anchored only by propane.

The practical implication is that renewable gaseous fuels should not be ranked by lower heating value alone. Biogas has lower energy density than methane because of its CO_2 fraction, but the same CO_2 fraction increases knock resistance and can enable higher compression ratio. Hydrogen enrichment can improve flame propagation and extend combustion control, but it may also change methane number and move the blend outside the calibration hull. Propane addition can increase energy density but may reduce knock margin and compression accessibility.

For engine design, this means that a fuel with lower heating value may still contain a valuable thermodynamic opportunity if it permits higher knock-limited compression. Conversely, a fuel with high energy density may be unattractive if the engine must retard spark or reduce effective compression to avoid knock.

4.8. Adaptive and Multifuel Engines

Gaseous-fuel performance is a fuel–engine–control interaction. Methane number, flame speed, dilution, energy density, H/C and γ° influence the knock-limited opportunity, but the share that is realized depends on compression ratio, spark timing, equivalence ratio, EGR, boost, chamber design, turbulence, heat losses and control strategy [15–17,38–40].

Future engines operating with variable gaseous fuels may use fuel-quality indicators or knock feedback to adjust compression ratio, spark timing, injection strategy, equivalence ratio, EGR, boost, valve timing or combustion phasing. In such adaptive engines, the same fuel could yield a different X_{fMN}. Therefore, the coefficients reported here should not be transferred directly. The transferable contribution is the methodology: construct the reference, measure the realized efficiency, compute the realization ratio and recalibrate within a declared domain. Variable displacement and compression ratio [12], cooled EGR [13] and in-cylinder-pressure-based knock detection [14] are examples of the means by which such adaptation can be implemented. The coefficients are also platform-specific: lean-burn, turbocharged, EGR-assisted or closed-loop knock-controlled engines change the effective specific-heat ratio, the burned-gas dilution and the end-gas state, so neither the magnitude nor the sign of the fitted γ_r exponent can be assumed to carry over to them.

4.9. Limitations and Future Work

The main limitation is the small BSI calibration set. Nine fuels are sufficient to reveal the methane-reference anchoring, denominator-driven behavior and non-identifiability of the full model, but they are not sufficient to establish a universal fuel-quality equation.

A second limitation concerns the nominal *MN* assignment of five engine blends: *MN* 105, 97, 66, 65 and 64. These nominal *MN* values belong to CFR mixtures of different compositions. With the *MN* that the thesis database lists for the engine compositions, the advantage over the null model disappears. Therefore, the 2.10× benchmark is conditional on the nominal *MN* assignment used in the source series.

A third limitation is that the biogas 60/40 point was measured with a high-turbulence piston configuration. Removing this point reduces the null-model improvement to 1.27×. Removing both extreme fuels reduces it to 0.77×.

A fourth limitation is that the thermochemical descriptors of the extended matrix are computed from compositions recovered from the thesis database, and record-level source information for *MN* is only partially documented.

A fifth limitation is that the repeatability/noise sensitivity uses the closest available repeatability proxy from *Energy* 2018—brake thermal efficiency at a single operating point and fuel blend—and should not be interpreted as a fuel-by-fuel uncertainty model for the nine calibration fuels.

A sixth limitation is that the lower part of the calibration hull, $\gamma^\circ < 1.24$, which covers about 40% of the hull area and is the only region where the model approaches or exceeds $X_{fMN} = 1$, is supported by a single fuel, propane (leverage $h = 0.88$; 77% of the variance of $\ln X_{fMN}$). Removing propane leaves the leave-one-out improvement at 2.12× (seven of eight fuels), but it removes the empirical anchor of that region.

External confirmation, as used in this paper, means more than applying the calibrated equation to additional compositions. It would require an independently measured dataset with (i) fuel composition and measured methane number or $CR_{crit,CFR}$ of the fuel actually burned; (ii) measured engine efficiency at the knock threshold or a clearly defined knock-limited operating condition; (iii) fuels not used in the present calibration; (iv) a documented engine configuration and operating protocol; and (v) the applicability-domain status of each case. Ideally it would be obtained on an independent platform or in an independent laboratory; on the same BSI platform, new fuels with newly measured efficiencies would still provide a valid out-of-sample test. The 84-record matrix is not external confirmation because measured efficiencies are not available for it.

Future work should focus on five directions:

1. Expanded BSI calibration with additional gaseous fuels, in particular hydrogen-enriched, highly diluted and propane-rich blends;

2. Variable-compression-ratio and adaptive spark-ignition platforms;
3. Advanced combustion strategies such as HCCI and RCCI;
4. Independent external confirmation with measured composition and *MN* of the fuel actually burned;
5. Real-time fuel-quality recognition and engine control unit (ECU)-based control for multifuel Otto engines.

5. Conclusions

This study reformulated X_{fMN} from a methane-normalized fuel-quality factor into a fuel–engine realization diagnostic referenced to a knock-limited Otto opportunity. The revised analysis separates the fuel-side knock rating, the thermodynamic reference and the measured electrical performance of a specific engine platform. This separation is important because gaseous fuels do not differ only in lower heating value or methane number; they also differ in thermodynamic response, dilution level, elemental composition and the extent to which a real engine can exploit their knock-limited potential.

1. The free-intercept reformulation resolves the methane-reference anchoring of the historical factor. The previous methane-normalized formulation imposed unity on methane by construction, whereas the measured BSI/Otto realization ratio for methane is approximately 0.544. Introducing a free intercept provides an algebraically consistent baseline and shows that the proposed factor should be interpreted as platform realization relative to a reference, not an absolute fuel-quality index.
2. The reduced two-descriptor model is the identifiable representation supported by the available nine-fuel calibration set. After methane number is used to construct the knock-limited Otto reference, the residual realization signal is captured by H/C and γ°. The full five-descriptor expression remains non-identifiable because the calibration set is small and the descriptors are strongly collinear. Therefore, the reduced model is not a reduction of the combustion physics but a regularized representation of what the available data can support.
3. The null-model benchmark is favorable only under the nominal methane-number assignment used in the source series. Under that assignment, the reduced model improves leave-one-out electrical efficiency prediction relative to the null model. However, assigning composition-consistent thesis methane numbers to five engine blends removes this advantage. The main predictive result must therefore be interpreted as conditional, local and dependent on the documented *MN*–composition pairing of the calibration fuels.
4. The applicability-domain analysis shows that most extended fuels require extrapolation. After reconstruction of the 84-record matrix, only 23 records lie inside the convex-hull interpolation domain, three are box-only cases and 58 are outside the supported region. The inside-hull and box-only projections reproduce the measured efficiency range, but they remain conditional projections rather than independent validation. The response surface shows that the calibrated model reaches values of X_{fMN} close to or above 1 only toward low γ° in a region that is supported by propane alone. This confirms that X_{fMN} should not be used to rank arbitrary gaseous fuels without declaring domain status.
5. The practical contribution is a diagnostic framework for fuel-adaptive gaseous-fuel engines. The reformulated factor separates the knock-limited thermodynamic opportunity from the measured platform realization. This makes it useful for evaluating how a specific spark-ignition engine, generator set or adaptive control strategy exploits the potential of methane, biogas, hydrogen-enriched blends, propane-containing blends and other gaseous fuels. Future work should focus on independent datasets with mea-

sured composition, *MN* or $CR_{crit,CFR}$, and efficiency at clearly defined knock-limited operating conditions.

Supplementary Materials: The following supporting information can be downloaded at: https://www.mdpi.com/article/10.3390/en19215374/s1, Workbook S1: XfMN_Figure_Data_Workbook_NIST-JANAF.xlsx (data behind Figures 1–7, sensitivity analyses and provenance sheets, including the sheet Fig7_Surface); Script S1: generar_figuras.py (Figures 1–6); Script S2: Figure7_surface.py (Figure 7 and its data sheet); Script S3: cantera_crosscheck.py (Cantera/GRI-Mech 3.0 cross-check).

Author Contributions: Conceptualization, J.P.G.M. and Y.C.A.; methodology, J.P.G.M., D.B.O., Y.C.A. and L.E.Q.G.; software, J.P.G.M., J.A.C.G., L.E.Q.G. and W.E.D.L.C.F.; validation, J.P.G.M., D.B.O., Y.C.A., J.A.C.G., L.E.Q.G., P.B.I.G. and W.E.D.L.C.F.; formal analysis, J.P.G.M., Y.C.A., J.A.C.G. and L.E.Q.G.; investigation, J.P.G.M., Y.C.A., P.B.I.G. and W.E.D.L.C.F.; resources, D.B.O.; data curation, J.P.G.M., D.B.O., J.A.C.G., P.B.I.G. and W.E.D.L.C.F.; writing—original draft preparation, J.P.G.M. and Y.C.A.; writing—review and editing, J.P.G.M., D.B.O., Y.C.A., J.A.C.G., L.E.Q.G., P.B.I.G. and W.E.D.L.C.F.; visualization, J.P.G.M., J.A.C.G., L.E.Q.G., P.B.I.G. and W.E.D.L.C.F.; supervision, D.B.O. and Y.C.A.; project administration, J.P.G.M. and Y.C.A. All authors have read and agreed to the published version of the manuscript.

Funding: This research received no external funding.

Institutional Review Board Statement: Not applicable.

Informed Consent Statement: Not applicable.

Data Availability Statement: The data, workbooks, scripts and figure-generation files supporting the results, including the script and the data sheet used to generate Figure 7, are provided as Supplementary Materials or are available from the corresponding author upon reasonable request.

Acknowledgments: The authors acknowledge the support of the Dirección de Investigación of Universidad Peruana de Ciencias Aplicadas through the UPC-EXPOST-2026-2 internal fund.

Conflicts of Interest: The authors declare no conflicts of interest.

Abbreviations and Symbols

The following abbreviations and symbols are used in this manuscript:

ATE 2025	Applied Thermal Engineering article of 2025 [21]
BSI	Biogas spark-ignition/high-compression spark-ignition test platform
CFR	Cooperative Fuel Research knock-rating engine
$CR_{crit,CFR}$	Critical compression ratio from CFR methane-number testing
COV_{IMEP}	Coefficient of variation of indicated mean effective pressure
CSU	Colorado State University
d_{hull}	Distance to the convex hull of the calibration fuels
ECM 2024	Energy Conversion and Management article of 2024 [20]
ECU	Engine control unit
ED°	Reference-condition energy density per stoichiometric air requirement
EGR	Exhaust gas recirculation
H/C	Elemental hydrogen-to-carbon ratio of the complete gaseous blend
h, h^{*}	Leverage and its Williams-type threshold
HCCI	Homogeneous charge compression ignition
IRLS	Iteratively reweighted least squares
K	Free multiplicative intercept of the realization model
KPP	Knock peak pressure
KT	Knock threshold
LHV	Lower heating value
LOO	Leave one out
MN	Methane number

OLS	Ordinary least squares
$P_{e,\max,KT}$	Maximum electrical power at the knock threshold
RCCI	Reactivity-controlled compression ignition
RMSE	Root-mean-square error
S_L°	Reference-condition laminar flame speed
T_{ad}°	Reference-condition adiabatic flame temperature
VIF	Variance inflation factor
X_{fMN}	Fuel–engine realization factor relative to a knock-limited Otto reference
γ°	Reference-condition specific-heat ratio
$\eta_{O,KL}^\circ$	Knock-limited Otto reference efficiency
$\eta_{e,KT}$	Measured electrical efficiency at the knock threshold
$\dot{E}_{fuel}$	Fuel energy input rate
κ	Condition number

References

1. Heywood, J.B. *Internal Combustion Engine Fundamentals*, 2nd ed.; McGraw-Hill Education: New York, NY, USA, 2018.
2. Zhen, X.; Wang, Y.; Xu, S.; Zhu, Y.; Tao, C.; Xu, T.; Song, M. The engine knock analysis—An overview. *Appl. Energy* **2012**, *92*, 628–636. [CrossRef]
3. Kalghatgi, G. Knock onset, knock intensity, superknock and preignition in spark ignition engines. *Int. J. Engine Res.* **2018**, *19*, 7–20. [CrossRef]
4. Kalghatgi, G.T. Fuel anti-knock quality—Part I: Engine studies. In *Proceedings of the SAE 2002 World Congress & Exhibition, Detroit, MI, USA, 4 March 2002; and SAE International Fall Fuels & Lubricants Meeting & Exhibition, San Antonio, TX, USA, 24 September 2001*; SAE Technical Paper 2001-01-3584; SAE International: Warrendale, PA, USA, 2001. [CrossRef]
5. Malenshek, M.; Olsen, D.B. Methane number testing of alternative gaseous fuels. *Fuel* **2009**, *88*, 650–656. [CrossRef]
6. *ASTM D8221*; Standard Practice for Determining the Calculated Methane Number of Gaseous Fuels Used in Internal Combustion Engines. Technical Report. ASTM International: West Conshohocken, PA, USA, 2019.
7. Gómez Montoya, J.P.; Amell, A.A.; Olsen, D.B. Prediction and measurement of the critical compression ratio and methane number for blends of biogas with methane, propane, and hydrogen. *Fuel* **2016**, *186*, 168–175. [CrossRef]
8. Poursadegh, F.; Brear, M.J.; Hayward, B.; Yang, Y. Autoignition, knock, detonation and the octane rating of hydrogen. *Fuel* **2023**, *332*, 126201. [CrossRef]
9. Gómez Montoya, J.P.; Amador, G.; Amell, A.A.; Olsen, D.B. Strategies to improve the performance of a spark ignition engine using fuel blends of biogas with natural gas, propane, and hydrogen. *Int. J. Hydrogen Energy* **2018**, *43*, 21592–21602. [CrossRef]
10. Kakaee, A.H.; Paykani, A.; Ghajar, M. The influence of fuel composition on the combustion and emission characteristics of natural gas fueled engines. *Renew. Sustain. Energy Rev.* **2014**, *38*, 64–78. [CrossRef]
11. Dal Forno Chuahy, F.; Splitter, D.; Boronat, V.; Wagnon, S.W. Enabling high compression ratio in boosted spark ignition engines: Thermodynamic trajectory and fuel chemistry effects on knock. *Combust. Flame* **2020**, *222*, 446–459. [CrossRef]
12. Rufino, C.H.; Ferreira, J.V. Study on the efficiency of a spark-ignition variable displacement and compression ratio engine. *Int. J. Engine Res.* **2021**, *22*, 2607–2621. [CrossRef]
13. Chaichan, M.T. Evaluation of the effect of cooled EGR on knock of SI engine fueled with alternative gaseous fuels. *Sulaimani J. Eng. Sci.* **2014**, *1*, 7–17. [CrossRef]
14. Kim, J. In-cylinder pressure based engine knock classification model for high-compression ratio, automotive spark-ignition engines using various signal decomposition methods. *Energies* **2021**, *14*, 3117. [CrossRef]
15. Yao, M.; Zheng, Z.; Liu, H. Progress and recent trends in homogeneous charge compression ignition (HCCI) engines. *Prog. Energy Combust. Sci.* **2009**, *35*, 398–437. [CrossRef]
16. Reitz, R.D.; Duraisamy, G. Review of high efficiency and clean reactivity controlled compression ignition (RCCI) combustion in internal combustion engines. *Prog. Energy Combust. Sci.* **2015**, *46*, 12–71. [CrossRef]
17. Milojević, S.; Stopka, O.; Kontrec, N.; Orynycz, O.; Hlatká, M.; Radojković, M.; Stojanović, B. Analytical characterization of thermal efficiency and emissions from a diesel engine using diesel and biodiesel and its significance for logistics management. *Processes* **2025**, *13*, 2124. [CrossRef]
18. Gómez Montoya, J.P.; Amell, A.A. Phenomenological analysis of the combustion of gaseous fuels to measure the energy quality and the capacity to produce work in spark ignition engines. *J. Eng. Gas Turbines Power* **2021**, *143*, 051016. [CrossRef]
19. Gómez Montoya, J.P.; Amell, A.A. Phenomenological analysis of the combustion of gaseous fuels to measure the fuel's energy quality and availability to produce work in spark ignition engines, Part 2. *J. Eng. Gas Turbines Power* **2022**, *144*, 051002. [CrossRef]

20. Gómez Montoya, J.P.; Olsen, D.B. A novel theory for designing SI engines based on exergy efficiency, entropy, octane rating, and fuels' physicochemical properties for Otto cycles. *Energy Convers. Manag.* **2024**, *322*, 119144. [CrossRef]
21. Gómez Montoya, J.P. A thermodynamic principle for engine design: Exergy optimization of spark-ignition engines fueled by hydrogen-enriched biogas based on Otto cycle foundations. *Appl. Therm. Eng.* **2025**, *280*, 128376. [CrossRef]
22. Gómez Montoya, J.P.; Olsen, D.B.; Amell, A.A. Engine operation just above and below the knock threshold using a blend of biogas and natural gas. *Energy* **2018**, *153*, 719–725. [CrossRef]
23. Gómez Montoya, J.P.; Amell, A.A. Effect of the turbulence intensity on knocking tendency in a spark ignition engine with high compression ratio using biogas and blends with natural gas, propane, and hydrogen. *Int. J. Hydrogen Energy* **2019**, *44*, 18532–18544. [CrossRef]
24. Gómez Montoya, J.P.; Amell, A.A.; Olsen, D.B. Operation of a spark ignition engine with high compression ratio using biogas blended with natural gas, propane, and hydrogen. *J. Eng. Gas Turbines Power* **2019**, *141*, 051006. [CrossRef]
25. Chase, M.W., Jr. *NIST-JANAF Thermochemical Tables*, 4th ed.; American Institute of Physics: Melville, NY, USA, 1998.
26. Linstrom, P.J.; Mallard, W.G. *NIST Chemistry WebBook, NIST Standard Reference Database Number 69*; National Institute of Standards and Technology: Gaithersburg, MD, USA, 2025. [CrossRef]
27. Barton, R.K.; Lestz, S.S.; Duke, L.C. Knock intensity as a function of engine rate of pressure change. In *Proceedings of the 1970 Automotive Engineering Congress and Exposition, Detroit, MI, USA, 12 January 1970*; SAE Technical Paper 700061; SAE International: Warrendale, PA, USA, 1970. [CrossRef]
28. Wise, D.M.; Olsen, D.B.; Kim, M. Characterization of methane number for producer gas blends. In *Proceedings of the ASME 2013 Internal Combustion Engine Division Fall Technical Conference, Dearborn, MI, USA, 13–16 October 2013*; Paper ICEF2013-19221, V002T02A015; American Society of Mechanical Engineers: New York, NY, USA, 2013. [CrossRef]
29. Kubesh, J.; King, S.; Liss, W. Effect of gas composition on octane number of natural gas fuels. In *Proceedings of the International Fuels & Lubricants Meeting & Exposition, San Francisco, CA, USA, 19 October 1992*; SAE Technical Paper 922359; SAE International: Warrendale, PA, USA, 1992. [CrossRef]
30. Arunachalam, A.; Olsen, D.B. Experimental evaluation of knock characteristics of producer gas. *Biomass Bioenergy* **2012**, *37*, 169–176. [CrossRef]
31. Amador, G.J.; Corredor, L.A.; Gómez Montoya, J.P.; Olsen, D.B. Methane number measurements of hydrogen/carbon monoxide mixtures diluted with carbon dioxide for syngas spark ignited internal combustion engine applications. *Fuel* **2019**, *236*, 535–543. [CrossRef]
32. Goodwin, D.G.; Moffat, H.K.; Schoegl, I.; Speth, R.L.; Weber, B.W. *Cantera: An Object-Oriented Software Toolkit for Chemical Kinetics, Thermodynamics, and Transport Processes*, Version 3.2.0; Zenodo: Geneva, Switzerland, 2025. [CrossRef]
33. Smith, G.P.; Golden, D.M.; Frenklach, M.; Moriarty, N.W.; Eiteneer, B.; Goldenberg, M.; Bowman, C.T.; Hanson, R.K.; Song, S.; Gardiner, W.C., Jr.; et al. *GRI-Mech 3.0*; Gas Research Institute: Chicago, IL, USA, 1999. Available online: http://www.me.berkeley.edu/gri_mech/ (accessed on 4 June 2026).
34. Netzeva, T.I.; Worth, A.P.; Aldenberg, T.; Benigni, R.; Cronin, M.T.; Gramatica, P.; Jaworska, J.S.; Kahn, S.; Klopman, G.; Marchant, C.A.; et al. Current status of methods for defining the applicability domain of (quantitative) structure–activity relationships. *Altern. Lab. Anim.* **2005**, *33*, 155–173. [CrossRef]
35. Sahigara, F.; Mansouri, K.; Ballabio, D.; Mauri, A.; Consonni, V.; Todeschini, R. Comparison of different approaches to define the applicability domain of QSAR models. *Molecules* **2012**, *17*, 4791–4810. [CrossRef]
36. O'Brien, R.M. A caution regarding rules of thumb for variance inflation factors. *Qual. Quant.* **2007**, *41*, 673–690. [CrossRef]
37. Belsley, D.A.; Kuh, E.; Welsch, R.E. *Regression Diagnostics: Identifying Influential Data and Sources of Collinearity*; John Wiley & Sons: New York, NY, USA, 1980.
38. Verhelst, S.; Wallner, T. Hydrogen-fueled internal combustion engines. *Prog. Energy Combust. Sci.* **2009**, *35*, 490–527. [CrossRef]
39. Wang, Z.; Liu, H.; Reitz, R.D. Knocking combustion in spark-ignition engines. *Prog. Energy Combust. Sci.* **2017**, *61*, 78–112. [CrossRef]
40. Christensen, M.; Johansson, B.; Einewall, P. Homogeneous charge compression ignition using iso-octane, ethanol and natural gas—A comparison with spark ignition operation. In *Proceedings of the International Fuels & Lubricants Meeting & Exposition, Tulsa, OK, USA, 13 October 1997*; SAE Technical Paper 972874; SAE International: Warrendale, PA, USA, 1997. [CrossRef]

Disclaimer/Publisher's Note: The statements, opinions and data contained in all publications are solely those of the individual author(s) and contributor(s) and not of MDPI and/or the editor(s). MDPI and/or the editor(s) disclaim responsibility for any injury to people or property resulting from any ideas, methods, instructions or products referred to in the content.